Directing exocrine secretory vesicles to the apical membrane by actin cables generated by the formin mDia1

Erez Geron, Eyal D. Schejter, and Ben-Zion Shilo[1]

Department of Molecular Genetics, Weizmann Institute of Science, Rehovot 76100, Israel

Edited by Thomas D. Pollard, Yale University, New Haven, CT, and approved May 1, 2013 (received for review February 28, 2013)

The final stage in exocrine secretion involves translocation of vesicles from their storage areas to the apical membrane. We show that actin-coated secretory vesicles of the exocrine pancreas travel this distance over bundles of specialized actin cables emanating from the apical plasma membrane. These bundles are stable structures that require constant G-actin incorporation and are distinct from the actin web that surrounds the exocrine lumen. The murine mammalian Diaphanous-related formin 1 (mDia1) was identified as a generator of these cables. The active form of mDia1 localized to the apical membrane, and introduction of an active form of mDia1 led to a marked increase in bundle density along the lumen perimeter. Compromising formation of the cables does not prevent secretion, but results in disorganized trafficking and fusion between secretory vesicles. Similar apical secretory tracks were also found in the submandibular salivary glands. Together with previous results that identified a role for Diaphanous in apical secretion in tubular organs of *Drosophila*, the role of Diaphanous formins at the final stages of secretion appears to be highly conserved.

actin polymerization | secretion tracks | pancreatic acini

Exocrine tissues such as the exocrine pancreas, the lacrimal glands and the salivary glands are professional secretory organs. They produce, store, and secrete proteins into a coalescing set of tubes. Exocrine tissues display a common morphological architecture, in which a few cells cluster to form a lobe that shares a joint lumen. These lobes are named acini ("grapes" in Latin), and each acinus is composed of 6–15 cells. Acinar cells form a highly polarized tubular epithelium. Such polarity is essential for generation of junctions between the cells and for directing secretion to the apical, luminal surface (1–3).

Pancreatic acinar cells contain hundreds of zymogen vesicles, which condense and mature along their trafficking route to the apical surface (4). These secretory vesicles are separated from the apical plasma membrane by a dense actin network, termed the "terminal web" (5, 6). In addition, several secretion-supporting roles have been assigned to subapical actin. Secretory vesicles undergo actin coating before fusing to the apical membrane, which has been implicated in vesicle stabilization and expulsion of vesicle content into the lumen (7–9). Finally, actin-dependent endocytosis has been shown to play a role in reducing lumen size following secretion and in recovering membrane material for generating new secretory vesicles (10). The difficulty of monitoring specific actin-based structures and the distinct and even opposing roles of these different structures have precluded a more detailed mechanistic understanding of the involvement of F-actin in secretion.

Previous work in our laboratory has identified a role for the formin Diaphanous (Dia) in tubular organs of *Drosophila* embryos. Dia is enriched at the apical membrane of these organs and generates apical F-actin cables, which are critical for trafficking secretory vesicles to the tubular organ lumen (11). Dia and its mammalian orthologs are dimeric, multidomain proteins (12). Upon activation by Rho GTPases, they generate linear actin filaments. In the absence of stimulation, interactions between the Dia inhibitory domain and the Dia autoregulatory domain (DAD) maintain Dia formins in an inactive, closed conformation. Rho-GTP binding to the GTPase binding domain of Dia relieves autoinhibition. The formin homology 1 (FH1) and DAD domains of dimerized Dia formins then deliver monomeric actin to the FH2 domains, which elongate and cap the barbed end of the actin filament (13).

Using live imaging of F-actin in pancreatic acinar cells, we identify a unique structure composed of actin cables. This structure is characterized by bundles of actin microfilaments emanating from the apical surface, which serve as tracks for transport of secretory vesicles. We propose that these structures are generated by the Dia-related formin mDia1. Activated mDia1 is targeted to the apical membrane of acinar cells, and expression of a constitutively active construct of mDia1 leads to an increase in density of the apical bundles. Compromising the formation of the cables, either by expression of a dominant-negative mDia1 construct or by treatment with latrunculin A (LatA) results in disorganized vesicle trafficking and fusion between them, although overall secretion persists. A central role for Dia-based apical actin cables in vesicle trafficking along the final leg of secretion appears to be an evolutionarily conserved feature, used by diverse secretory organs across different phyla.

Results

Short-Range Transport of Secretory Vesicles over Apical F-Actin Bundles in Exocrine Pancreatic Acinar Cells. To study actin dynamics during exocrine secretion, we used primary cultures of pancreatic acini. In this setup, the murine pancreas is excised and enzymatically digested to yield isolated acini (14). To follow F-actin dynamics, we used adenoviral infection to introduce Lifeact-GFP (15), an F-actin probe, into dispersed acini. This tool allowed us to follow the dynamics of F-actin during pancreatic secretion for up to 16 h after infection, at a level of resolution that could not be attained in fixed acinar samples (Fig. 1). In addition, use of the Lifeact-GFP probe allowed simultaneous visualization of secretory vesicles, as pancreatic zymogen vesicles undergo actin coating shortly before exocytosis (7–9).

During live imaging, the apical region of pancreatic acinar cells was identified by its dense concentration of F-actin and by the orientation of fusing vesicles, which move concentrically in adjacent cells toward their joint lumen (Fig. 1 and Movies S1, S2, and S3). General labeling of cell membranes with a lipophilic dye demonstrates that the apical surface is highly restricted and occupies only a small fraction of the cell circumference (Fig. 1*B* and Movie S1).

Author contributions: E.G., E.D.S., and B.-Z.S. designed research; E.G. performed research; E.G., E.D.S., and B.-Z.S. contributed new reagents/analytic tools; E.G., E.D.S., and B.-Z.S. analyzed data; and E.G., E.D.S., and B.-Z.S. wrote the paper.

The authors declare no conflict of interest.

This article is a PNAS Direct Submission.

[1]To whom correspondence should be addressed. E-mail: Benny.Shilo@Weizmann.ac.il.

This article contains supporting information online at www.pnas.org/lookup/suppl/doi:10.1073/pnas.1303796110/-/DCSupplemental.

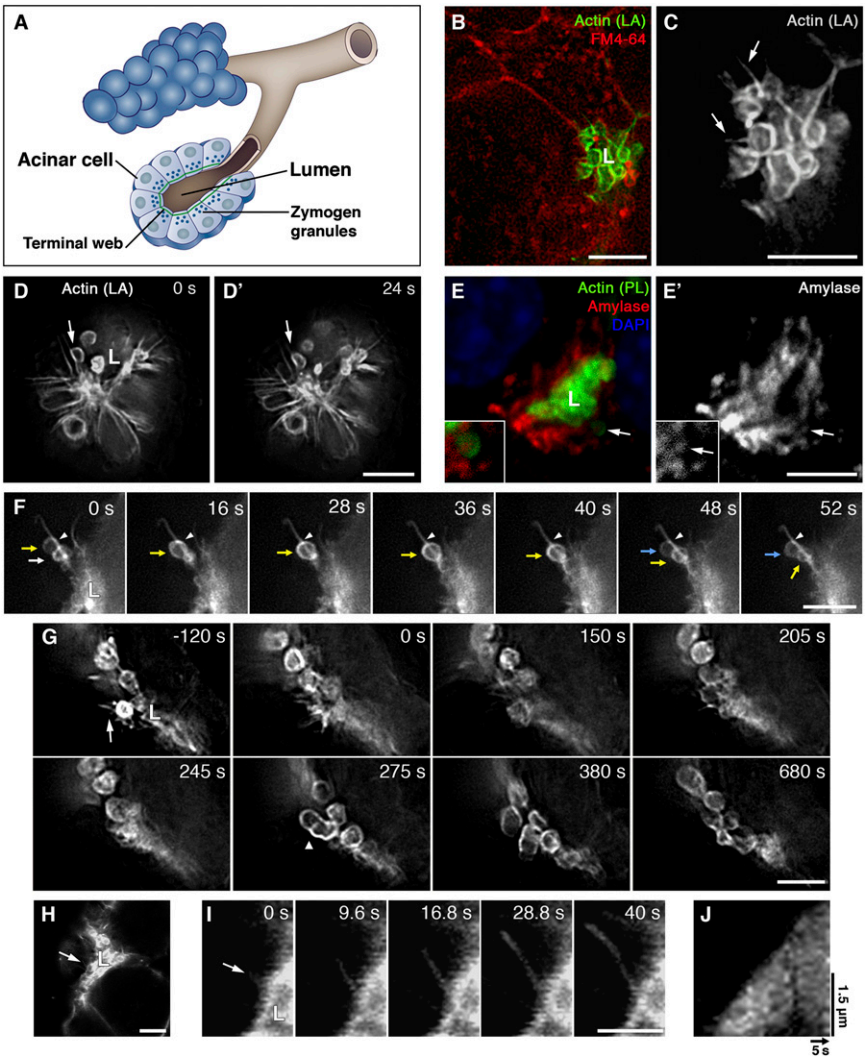

Fig. 1. Short-range transport of secretory vesicles over apical F-actin bundles in pancreatic acinar cells. (*A*) Illustration of pancreatic acini. Note the joint apical lumen formed by a few acinar cells and the actin terminal web at its circumference. (*B* and *C*) Live stimulated acinar cells expressing Lifeact-GFP (LA; green, gray) and stained with the lipophilic dye FM4-64 (red). Cells were infected overnight with Ad-Lifeact-GFP, stained, and stimulated briefly with 100 pM CCK before the initiation of imaging. "L" marks the lumen in this and subsequent panels and figures. *C* is an enlargement of the lumen shown in *B*. Arrows point to F-actin bundles. (*D* and *D′*) Time series of acinar cells expressing Lifeact-GFP, stimulated with 100 pM CCK. Arrows point to an F-actin bundle with a closely associated actin-coated vesicle. (*E* and *E′*) Visualization of acinar components following stimulation and fixation. Acini were isolated and left to recover for 30 min, stimulated with CCK for 10 min, and fixed. Amylase-containing vesicles (red, gray) cluster near the lumen, which is lined with phalloidin-labeled F-actin (green). Nuclei are labeled with DAPI (blue). Note the single amylase vesicle coated with actin in the vicinity of the lumen (arrow), magnified (×1.5) in the insets. (*F*) Time series of actin-coated vesicles moving over a single actin bundle. Arrows of different colors indicate distinct actin-coated vesicles moving sequentially along an actin bundle. Arrowheads indicate the position of the upper vesicle (yellow arrow) at t = 0 s. (*G*) Similar CCK-stimulated acini during exposure to LatA (1 μM), which was added at t = 0 s. The arrow (at −120 s) indicates an F-actin bundle. These structures disappear following treatment with LatA. The arrowhead (at 275 s) points to a compound secretion event. (*H–J*) De novo growth of an actin bundle. The time-lapse series in *I* depicts the growth of the bundle (arrow). The kymograph in *J*, plotted along the line of bundle growth so that the apical surface corresponds with the image base, shows the constant rate of cable elongation. [Scale bars, 5 μm (*B–H*), 2.5 μm (*I*), and 1.5 μm (*J*).]

Using the Lifeact-GFP probe, we observed and characterized unique, fine structures of bundled F-actin cables emanating from the apical surface of pancreatic acinar cells (Fig. 1 *B–D′* and Movies S1 and S2). Each bundle extends from a single apical anchorage point inward into the cell. The bundles reach an average length of 3.6 ± 0.9 μm, and the bundle density along the lumen perimeter is 9.6 ± 4.2 bundles per 20 μm (n = 20 lumens). Bundle width cannot be measured accurately, because it is below the resolution limit of the microscope (~0.25 μm). The bundles were barely detectable in fixed samples by fluorescent phalloidin, the conventional probe for F-actin (Fig. S1).

The apical domain of an acinar cell is packed with hundreds of secretory vesicles, only a small fraction of which undergoes exocytosis following stimulation (Fig. 1 *E* and *E′*) (5). By live tracking of actin-coated vesicles, it was possible to monitor individual exocytosis events. Secretion was triggered by addition of 100 pM cholecystokinin (CCK) immediately before imaging. Time-lapse imaging of CCK-stimulated acini showed that actin-coated vesicles moved directionally toward the apical surface, and many of them were closely associated with the actin bundles (Fig. 1*D* and Movies S2 and S3). Closer examination revealed that pancreatic vesicles follow the bundle outline and move along it toward the lumen without detaching (Fig. 1*F* and Movie S4). Actin-coated vesicles traversed over the bundles an average distance of 1.6 ± 0.4 μm, at an average speed of 34.6 ± 10.3 nm/s (n = 40). Each vesicle traveled over a single bundle. Conversely,

individual bundles served as tracks for two or more vesicles, even within a short time window of ~30 s (Fig. 1*F* and Movie S4). Once vesicles reached the apical membrane, fusion occurred primarily through a single fusion event (Fig. 1 *B–F* and Movies S1, S2, S3, and S4) (16).

Apical Actin Bundles Are Stable Structures with a Rapid Turnover. The apical bundles appeared to be stable structures that retain a constant length over long imaging periods (>30 min). We therefore sought to determine whether they represent static or dynamic structures. We interfered with actin polymerization by exposing dispersed acini to the G-actin sequestering agent LatA. A moderate dosage (1 μM) of LatA was used to avoid global and adverse effects (see below).

A prominent change that followed actin sequestration was the rapid disappearance of the apical bundles (Fig. 1*G* and Movie S5). Within 5 min of LatA addition, no apical actin bundles were detected (Fig. 1*G* and Movie S5). These results indicate that the apical bundles are sensitive to the availability of G-actin and require constant incorporation of actin monomers into their filaments. Other actin structures were more stable. For example, F-actin surrounding the vesicles was still apparent, even 10 min after LatA addition.

The persistence of actin coating allowed us to monitor secretory vesicles following elimination of the actin bundles, and therefore to assess the significance of these structures to the secretory process. A notable alteration in vesicle behavior was observed. Instead of reaching and directly fusing with the apical cell membrane, nearly half (47.7 ± 5.4%) of the vesicles fuse into other vesicles that are partially fused to the apical surface ($n = 89$ fusion events, from four different lumens visualized in three independent experiments) (Fig. 1*G* and Movie S5). This fusion phenotype, known as "compound secretion," is increased dramatically compared with nontreated cells, in which only a minority (13.2 ± 7.2%) of the actin-coated vesicles fuse with one another ($n = 100$ fusion events, from nine different lumens visualized in seven independent experiments). We propose that this alteration in fusion profile results from the loss of apical actin cables, compromising the efficiency of orderly targeting of vesicles to the apical plasma membrane. The secretion of amylase to the medium was not significantly affected following a short incubation with LatA, implying that the compound secretion bodies can expel their content into the lumen. Interestingly, an intravital study of regulated secretion in acinar cells of murine salivary glands reported a similar fusion pattern shift following treatment with inhibitors of F-actin polymerization (17).

To monitor the directionality and rate of actin flow in the apical bundles, we recorded a rare event of de novo bundle growth (Fig. 1 *H–J* and Movie S6). Growth of the bundle initiated at the apical surface and advanced inward toward the cytoplasm (Fig. 1 *H–J* and Movie S6). The bundle reached a final length of 2.7 μm following 36.1 s of growth, at an average rate of 7.5 nm/s. A kymograph plot of this event demonstrates that bundle growth proceeds at a constant rate of elongation (Fig. 1*J*).

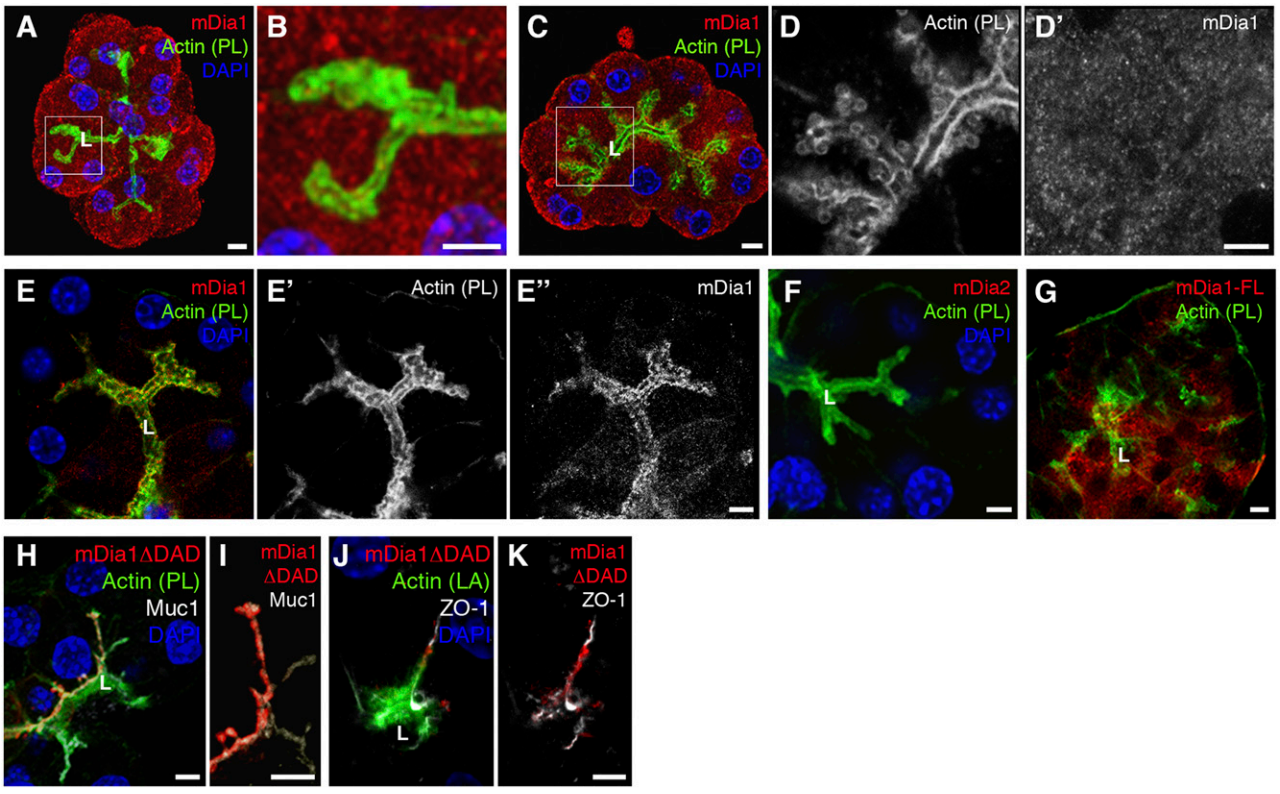

Fig. 2. mDia1 localization in pancreatic acinar cells. (*A–D'*) Localization of endogenous mDia1 (red, gray in *D'*) in the absence (*A*, enlarged in *B*) or presence (*C*, enlarged in *D* and *D'*) of CCK stimulation. F-actin is visualized with phalloidin (PL; green, gray in *D*) and nuclei with DAPI (blue). (*E–E''*) Apical membrane-associated localization of mDia1 (red, gray) is revealed by cytoplasmic clearance. (*F*) mDia2 (red) is absent from pancreatic acinar cells. (*G–K*) Localization of adenoviral-delivered mDia1 constructs. Acini were infected with viruses harboring either mDia1-FL-Myc (*G*) or mDia1ΔDAD-Myc (*H–K*). Acini were then washed, fixed, and stained. Localization of the mDia constructs was revealed using anti-Myc antibodies (red). Although the full-length construct is generally dispersed (*G*), the mDia1ΔDAD-Myc construct is found close to the apical markers Muc1 (*H* and *I*) and ZO-1 (*J* and *K*) (gray), and to the apical F-actin (green). (Scale bars, 5 μm.)

Apical Localization of Active mDia1 in Pancreatic Acinar Cells. Next, we were interested in identifying the cellular machinery that generates the apical actin bundles in pancreatic acinar cells. Previous work from our laboratory demonstrated a role for the formin Dia in generation of actin cables that promote secretion from tubular organs of the *Drosophila* embryo (11). We thus considered mDia proteins, the mammalian orthologs of Dia, as candidates for formation and maintenance of apical actin bundles in acinar cells. Immunofluorescent localization using specific antibodies revealed pronounced expression of mDia1 in acinar cells, but failed to detect expression of mDia2 in these cells (Fig. 2*A* and *F*, respectively).

mDia1 exhibited a general cytoplasmic distribution in the acinar cells, irrespective of CCK stimulation (Fig. 2 *A–D′*). However, subjecting the cells to cytoplasmic clearance by permeabilization during the fixation process revealed an apically localized fraction of the endogenous mDia1 protein (Fig. 2 *E–E′′*). These observations raised the possibility that an active fraction of mDia1 proteins is apically localized in acinar cells, and is masked by the uniform distribution of autoinhibited molecules (18). To address this issue, we used adenoviral infection to express in pancreatic acini mDia1ΔDAD, a constitutively active form lacking the inhibitory C-terminal domain, and we monitored its localization. In contrast to the full-length construct mDia1-FL (Fig. 2*G*), which like endogenous mDia1 exhibits a uniform distribution, mDia1ΔDAD localized exclusively to the apical plasma membrane, close to the subapical actin layer and to the luminal markers mucin 1 (Muc1) and zona occludens 1 (ZO-1) (Fig. 2 *H–K*).

Apical Actin Bundles Are Generated by mDia1. The apical localization of activated mDia1 within acinar cells suggests a causal role in the formation of the actin bundles. To substantiate this relationship, we first assessed the effect of elevated mDia1 activity on the density of apical actin bundles. To this end, an adenovirus harboring the constitutively active mDia1ΔDAD construct was used, along with adenovirus (Ad)-Lifeact-GFP, to coinfect dispersed acini. Infections were carried out at a ratio in which most cells expressing Lifeact-GFP were also infected with the activated mDia1 construct. Control acini were similarly coinfected by Ad-Lifeact-GFP and Ad-red fluorescent protein (RFP).

The apical bundle density was calculated by dividing the number of actin bundles by the length of the lumen perimeter, in lumens formed by three or more Lifeact-GFP–expressing cells, and displaying at least two bundles. When comparing bundle density in control acini with those infected with activated mDia1, a significant difference was observed. While the average density of bundles along the lumen perimeter of control acini was 9.6 ± 4.2 bundles per 20 μm (n = 20 lm), following expression of mDia1ΔDAD the density was increased to 15.9 ± 5.8 bundles per 20 μm (n = 22 lumens, $P = 3.9 \times 10^{-3}$) (Fig. 3*A*).

To examine whether mDia1 is essential for formation of the actin bundles, we compromised the endogenous activity by infecting the acinar cells with an adenovirus expressing mDia1ΔDAD-I845A, a potent dominant-negative form of mDia1 (19). This variant bears a substitution of isoleucine at residue 845 to alanine, and was shown to abolish mDia1 actin polymerization activity (19). Pancreatic acini coinfected with the I845A mDia1 construct, along with Ad-Lifeact-GFP, showed a significantly reduced number of apical actin bundles (3.3 ± 2.6 bundles per 20 μm, n = 15 lumens, $P = 2.1 \times 10^{-3}$). In addition, expression of the mDia1 dominant-negative construct led to a pronounced increase in the incidence of compound secretion (39.9 ± 13.3% of total fusion events, n = 113 fusion events, from 12 different lumens visualized in five independent experiments) (Fig. 3 *B* and *C* and Movie S7). This observation is in line with the fusion profile alteration that followed the abolishment of the apical bundles by LatA treatment (Figs. 1*G* and 3*B*). Similar to the short LatA treatment, the overall level of amylase secretion was not significantly altered (Fig. 3*D*).

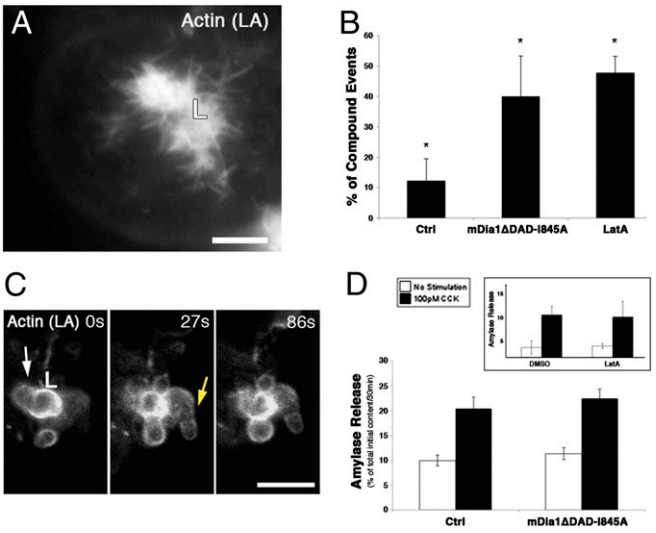

Fig. 3. mDia1 activity affects the density of apical actin bundles and the coordination of vesicle transport. (*A*) Expression of a constitutively active form of mDia1 leads to an increased density of apical actin bundles. Live acinar cells were coinfected with Lifeact-GFP (LA; gray) and mDia1ΔDAD for 16 h before imaging. (Scale bar, 5 μm.) (*B*) Percentage of compound fusion events out of total events. Pancreatic acini were isolated and infected with Lifeact-GFP for 16 h to enable visualization of microfilament structures. The acini were then washed and stimulated with 100 pM CCK immediately before imaging, which allowed monitoring of vesicle fusion events, either directly with the cell surface or with compound structures (Ctrl column). A portion of the acini was coinfected with adenoviruses harboring a dominant-negative construct of mDia1 (mDia1ΔDAD-I845A column), and a second portion was treated with 1 μM LatA several minutes after the onset of imaging (LatA column). Results represent the average and SD of 89–113 fusion events from four to seven independent experiments; $P = 1.8 \times 10^{-5}$ and $P = 1 \times 10^{-6}$, respectively. (*C*) Time-lapse series of pancreatic acinar cells coinfected with Ad-Lifeact-GFP and Ad-mDia1ΔDAD-I845A stimulated with CCK and depicting compound secretion events (arrows point to two such events). (Scale bar, 5 μm.) (*D*) Amylase release from acini that were infected with either a control virus (Ad-RFP) or with adenoviruses harboring the mDia1ΔDAD-I845A construct. CCK (100 pM) was added and medium collected after 30 min, to monitor amylase secretion. Results represent the average and SEM of four independent experiments. (*Inset*) Amylase release from freshly isolated acini treated with DMSO (1 mg/mL) or LatA (1 μM). Acini were isolated and left to recover for 30 min. Acini were then preincubated for 15 min with the indicated reagents and further incubated in the presence of these reagents, with or without optimal CCK concentration (50 pM) (Fig. S3), for 30 min. Medium collected following the final incubation period was used to monitor amylase release.

We note that the mDia1ΔDAD-I845A construct did not abolish actin coating around secretory vesicles (Fig. 3*C*). Both actin-related protein 3 (Arp3), a subunit of the Arp2/3 complex, and the Arp2/3 activator *N*-WASp (Neural Wiskott–Aldrich syndrome protein), are highly enriched around actin-coated vesicles (Fig. S2 *A* and *B*, respectively). These observations suggest that in acinar cells, actin coating of secretory vesicles may be mediated by the branched actin nucleation machinery.

Actin Bundles in Submandibular Salivary Acinar Cells. The presence of actin secretion tracks generated by Dia formins in various tubular organs of the fly and in the murine pancreas suggests that this mechanism may be used by a broad range of exocrine tissues. We chose to test whether this molecular machinery is operating in a second mammalian secretory organ, the submandibular salivary glands. Similar to the exocrine pancreas, the acinar structures of these glands can be stimulated by CCK or isoproterenol, and exhibit a prominent subapical layer of actin microfilaments. We thus could use the same ex vivo setup used for pancreatic acini to

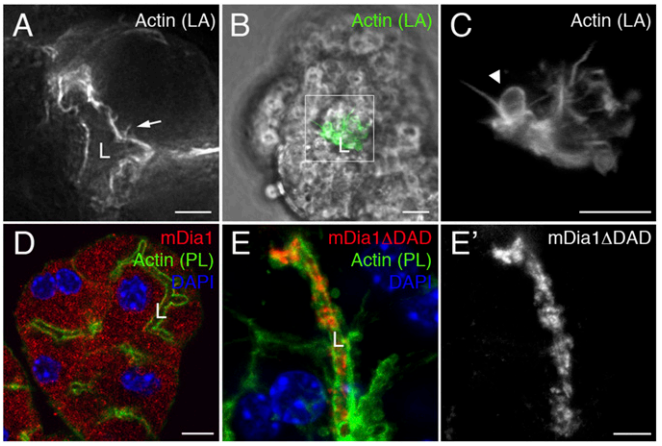

Fig. 4. Actin bundles and mDia1 in submandibular salivary gland acinar cells. (*A–C*) Live images of acinar cells of murine submandibular salivary glands expressing Lifeact-GFP. Cells were infected overnight with Ad-Lifeact-GFP and stimulated with CCK briefly before imaging. (*A*) Lifeact-GFP (gray) marks the apical actin web surrounding the lumen and associated actin cables (arrow). (*B*) Combined transmitted-light (gray) and Lifeact-GFP (green) image showing the actin-rich lumen of a salivary gland. (*C*) Enlargement of the boxed region in *B*, showing actin structures (gray) in the vicinity of the lumen. The arrowhead points to an actin-coated vesicle associated with an actin bundle. (*D*) Localization of endogenous mDia1 (red) in submandibular salivary acini. Acini were fixed 30 min after isolation. Phalloidin labels F-actin structures (green), and nuclei are labeled with DAPI (blue). (*E* and *E′*) The localization pattern of mDia1ΔDAD-Myc (anti-myc; red, gray in *E′*) was visualized following viral infection of this activated construct. Cells were stained as in *D*. (Scale bars, 5 μm.)

assess apical actin organization and mDia1 function in this second secretory organ.

Remarkably, apical actin bundles could be visualized in stimulated salivary acini that were infected with the Ad-Lifeact-GFP virus (Fig. 4 *A–C*). As in pancreatic secretion, salivary vesicles undergo actin coating and were found in close association with the apical actin bundles (Fig. 4 *B* and *C*). We next turned to visualize mDia1 localization in these glands. Here again, endogenous mDia1 exhibited a broad cytoplasmic distribution (Fig. 4*D*), whereas the constitutively active form mDia1ΔDAD, introduced via adenoviral infection, localized prominently to the apical membrane (Fig. 4 *E* and *E′*). This series of observations closely recapitulates those made in the pancreatic system, and therefore is consistent with a general role for mDia1 in generating F-actin bundles that coordinate the orderly transport of secretory vesicles to the apical membrane.

Discussion

The apical bundles of filamentous actin reported here constitute a unique F-actin structure in acinar cells. Our data suggest that these actin bundles are generated by the formin mDia1, as mDia1 is localized at the apical membrane and bundle density is correlated with mDia1 activity. Importantly, we observe a close association of secretory vesicles with the actin cables, and apparent movement of the vesicles on the cables immediately before their fusion with the plasma membrane.

Involvement of the mDia1-dependent cables in guiding exocrine secretion is suggested by the abnormal behavior of secretory vesicles in cultured pancreatic acini, when cable formation is compromised either through treatment with LatA or following expression of a dominant-negative form of mDia1. Under these circumstances, secretory vesicles, which normally fuse individually with the apical cell surface, are likely to fuse with each other and generate compound, membrane-associated secretory structures. Such compound fusion can be achieved by transfer of fusion components from the apical membrane to exocytosing vesicles, which then serve as extensions of the apical membrane into the granular area (20, 21). Secretion levels appear unaffected, implying that the compound structures can still secrete their contents to the lumen. The actin cables therefore perform an organizational role in this setting, ensuring orderly fusion of single secretory vesicles to the apical cell membrane.

The manner by which secretory vesicles move over the apical actin cables remains an open question. One possibility is that the vesicles are indirectly "transported" following myosin II-based contraction of the actin network at the apical cell surface. An alternative mechanism is direct transport along the cables via unconventional myosin motors, such as myosin V (Fig. 5). We favor such a mechanism, because myosin V family motors have been shown to mediate secretory vesicle transport both in *Saccharomyces cerevisiae*, in which actin cables generated by the formin Bni1-related1 (Bnr1), located at the bud neck, serve as tracks for vesicle transport to the growing bud (22), and in our previous study of secretion via Dia-generated cables in *Drosophila* tubular organs (11). Furthermore, the velocity of vesicle movement over actin bundles that we report is similar to the measured velocity of vesicle transport via myosin Vc, the predominant myosin V isoform in the exocrine pancreas (23, 24).

In conclusion, our studies demonstrate a role for Dia-family actin nucleators in generating apical actin structures in secretory organs of mice and flies. We propose that these actin structures coordinate the final stages of vesicle secretion in those physiological settings.

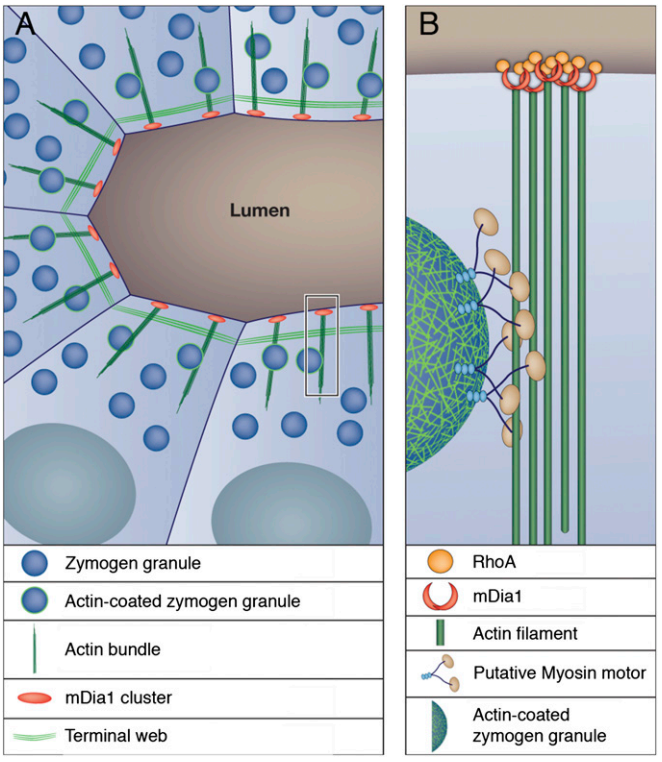

Fig. 5. Model for apical secretion in exocrine organs. (*A*) Exocrine acinar cells display three distinct types of subapical F-actin: branched-actin–coated vesicles; linear actin bundles, which we propose serve as tracks for transport of the actin-coated vesicles to the apical membrane; and a terminal web of actin that restricts nonregulated secretion. (*B*) Enlargement of the boxed region in *A*. Movement of actin-coated vesicles over the apical actin bundles may be mediated by unconventional myosin motor proteins. mDia1-dependent actin cable growth is initiated at the cell surface, possibly via activation by membrane-anchored RhoA.

Materials and Methods

Isolation and Culture of Acini. All experiments on mice were approved by the Weizmann Institute of Science committee for animal experimentation. Dispersed mouse pancreatic and salivary acini were prepared as described previously (25). In brief, Institute for Cancer Reseach (ICR) mice were euthanized according to institutional animal care guidelines, and their pancreata or submandibular salivary glands were excised. Excised tissues were minced to 1–3-mm pieces and digested for ~10 min in oxygenized Krebs-Ringer buffer (KRB) medium supplemented with 0.5 mg/mL BSA and 0.1 mg/mL soybean trypsin inhibitor (STI) (resuspension medium) and with collagenase XI (0.75 mg/mL). The digested tissues were washed with resuspension medium and filtered first through a coarse mesh, then through a 100-μm nylon mesh. The exocrine acini were allowed to settle on the bottom of 15-mL tubes, a step that was repeated two to three times to remove floating, damaged acini. For overnight culturing, acini were resuspended in DMEM supplemented with FCS (5% volume), sodium pyruvate (1%), antibiotics (1%), L-glutamine (0.5%), BSA (10 mg/mL), and STI (0.2 mg/mL). Acini were plated at low density on plates coated with 5 μg/mL collagen IV for 5 h and were incubated at 37 °C in 5% CO_2 humidified air. Acini were infected with 10^6 pfu/mL for 9–16 h before examination. In cases of coinfection, a final titer of 10^7 pfu/mL was used. Live-imaging experiments were carried out at 37 °C in resuspension medium. Cultured/infected acini had retained their in vivo polarity and amylase secretion pattern. Experiments were conducted with acini from a single pancreas or from a pair of submandibular salivary glands. Mice were handled according to the institutional animal care and use committee guidelines.

Immunohistochemical Preparation. Fresh or incubated acini were incubated in the presence or absence of 50–100 pM CCK for 5–15 min and fixed in 4% paraformaldehyde (PFA) in PBS for 20 min. Fixed acini were then washed extensively in PBS supplemented with 0.6% Triton X-100 and blocked for 30 min with CAS-Block (Invitrogen). Acini were then incubated with the indicated primary antibodies diluted in CAS-Block overnight at 4 °C, washed, and incubated with the appropriate secondary antibodies and with DAPI for 45 min at room temperature. Where indicated, FITC- or TRITC-phalloidin was added along with the secondary antibody for intracellular staining of F-actin. Lifeact-GFP was visualized after fixation by GFP fluorescence. Acini were then washed, resuspended in an 80% glycerol/20% PBS mix, and mounted for viewing. For cytoplasmic clearance, cells were fixed and permeabilized in 4% PFA, 0.5% Triton, and 5% sucrose in PBS for 4 min, washed and fixed again in 4% PFA and 5% sucrose in PBS for 25 min.

Microscopy. Data were acquired with either a DeltaVision system (Applied Precision), consisting of an inverted microscope IX71 equipped with 60×/1.4 or 100×/1.3 objectives (Olympus), or LSM510 and LSM710 confocal microscopes equipped with 60×/1.4 or 100×/1.4 objectives (Zeiss). Figs. 1 *D*, *F*, and *G* and 4*A* were subjected to digital deconvolution (enhanced ratio) with Softworx software (Applied Precision).

ACKNOWLEDGMENTS. We thank T. Rousso and the other members of the B.-Z.S. laboratory for fruitful input, Y. Dor for discussions, J. Magenheim and A. Swisa for technical advice, and O. Issler for continuous help. This work was supported by a US–Israel Binational Science Foundation grant to E.D.S. and B.-Z.S. and by a Schoenheimer Foundation grant to B.-Z.S., who is an incumbent of the Hilda and Cecil Lewis Chair in Molecular Biology.

1. Motta PM, Macchiarelli G, Nottola SA, Correr S (1997) Histology of the exocrine pancreas. *Microsc Res Tech* 37(5-6):384–398.
2. Williams JA (2006) Regulation of pancreatic acinar cell function. *Curr Opin Gastroenterol* 22(5):498–504.
3. Bryant DM, Mostov KE (2008) From cells to organs: Building polarized tissue. *Nat Rev Mol Cell Biol* 9(11):887–901.
4. Palade G (1975) Intracellular aspects of the process of protein synthesis. *Science* 189(4200):347–358.
5. Wäsle B, Edwardson JM (2002) The regulation of exocytosis in the pancreatic acinar cell. *Cell Signal* 14(3):191–197.
6. Williams JA, Chen X, Sabbatini ME (2009) Small G proteins as key regulators of pancreatic digestive enzyme secretion. *Am J Physiol Endocrinol Metab* 296(3):E405–E414.
7. Nemoto T, Kojima T, Oshima A, Bito H, Kasai H (2004) Stabilization of exocytosis by dynamic F-actin coating of zymogen granules in pancreatic acini. *J Biol Chem* 279(36): 37544–37550.
8. Valentijn JA, Valentijn K, Pastore LM, Jamieson JD (2000) Actin coating of secretory granules during regulated exocytosis correlates with the release of rab3D. *Proc Natl Acad Sci USA* 97(3):1091–1095.
9. Nightingale TD, Cutler DF, Cramer LP (2012) Actin coats and rings promote regulated exocytosis. *Trends Cell Biol* 22(6):329–337.
10. Valentijn KM, Gumkowski FD, Jamieson JD (1999) The subapical actin cytoskeleton regulates secretion and membrane retrieval in pancreatic acinar cells. *J Cell Sci* 112(Pt 1):81–96.
11. Massarwa R, Schejter ED, Shilo BZ (2009) Apical secretion in epithelial tubes of the Drosophila embryo is directed by the Formin-family protein Diaphanous. *Dev Cell* 16(6):877–888.
12. Maiti S, et al. (2012) Structure and activity of full-length formin mDia1. *Cytoskeleton (Hoboken)* 69(6):393–405.
13. Chesarone MA, DuPage AG, Goode BL (2010) Unleashing formins to remodel the actin and microtubule cytoskeletons. *Nat Rev Mol Cell Biol* 11(1):62–74.
14. Williams JA, Korc M, Dormer RL (1978) Action of secretagogues on a new preparation of functionally intact, isolated pancreatic acini. *Am J Physiol* 235(5):517–524.
15. Riedl J, et al. (2008) Lifeact: A versatile marker to visualize F-actin. *Nat Methods* 5(7):605–607.
16. Behrendorff N, Dolai S, Hong W, Gaisano HY, Thorn P (2011) Vesicle-associated membrane protein 8 (VAMP8) is a SNARE (soluble N-ethylmaleimide-sensitive factor attachment protein receptor) selectively required for sequential granule-to-granule fusion. *J Biol Chem* 286(34):29627–29634.
17. Masedunskas A, et al. (2011) Role for the actomyosin complex in regulated exocytosis revealed by intravital microscopy. *Proc Natl Acad Sci USA* 108(33):13552–13557.
18. Ramalingam N, et al. (2010) Phospholipids regulate localization and activity of mDia1 formin. *Eur J Cell Biol* 89(10):723–732.
19. Harris ES, Rouiller I, Hanein D, Higgs HN (2006) Mechanistic differences in actin bundling activity of two mammalian formins, FRL1 and mDia2. *J Biol Chem* 281(20): 14383–14392.
20. Pickett JA, Thorn P, Edwardson JM (2005) The plasma membrane Q-SNARE syntaxin 2 enters the zymogen granule membrane during exocytosis in the pancreatic acinar cell. *J Biol Chem* 280(2):1506–1511.
21. Sokac AM, Bement WM (2006) Kiss-and-coat and compartment mixing: Coupling exocytosis to signal generation and local actin assembly. *Mol Biol Cell* 17(4): 1495–1502.
22. Chesarone M, Gould CJ, Moseley JB, Goode BL (2009) Displacement of formins from growing barbed ends by bud14 is critical for actin cable architecture and function. *Dev Cell* 16(2):292–302.
23. Rodriguez OC, Cheney RE (2002) Human myosin-Vc is a novel class V myosin expressed in epithelial cells. *J Cell Sci* 115(Pt 5):991–1004.
24. Marchelletta RR, Jacobs DT, Schechter JE, Cheney RE, Hamm-Alvarez SF (2008) The class V myosin motor, myosin 5c, localizes to mature secretory vesicles and facilitates exocytosis in lacrimal acini. *Am J Physiol Cell Physiol* 295(1):C13–C28.
25. Gautam D, et al. (2005) Cholinergic stimulation of amylase secretion from pancreatic acinar cells studied with muscarinic acetylcholine receptor mutant mice. *J Pharmacol Exp Ther* 313(3):995–1002.